Molecular Model with Quantum Mechanical Bonding Information

3 AUTHORS, INCLUDING:

Hugo Javier Bohorquez
Fundación instituto de Inmunología de Colo…
16 PUBLICATIONS **175** CITATIONS

Russell J Boyd
Dalhousie University
**304** PUBLICATIONS **6,008** CITATIONS

Molecular Model with Quantum Mechanical Bonding Information

Hugo J. Bohórquez,*,[†] Russell J. Boyd,[†] and Chérif F. Matta[‡]

[†]Department of Chemistry, Dalhousie University, Halifax, Nova Scotia, Canada B3H 4R2

[‡]Department of Chemistry and Physics, Mount Saint Vincent University, Halifax, Nova Scotia, Canada B3M 2J6

ABSTRACT: The molecular structure can be defined quantum mechanically thanks to the theory of atoms in molecules. Here, we report a new molecular model that reflects quantum mechanical properties of the chemical bonds. This graphical representation of molecules is based on the topology of the electron density at the critical points. The eigenvalues of the Hessian are used for depicting the critical points three-dimensionally. The bond path linking two atoms has a thickness that is proportional to the electron density at the bond critical point. The nuclei are represented according to the experimentally determined atomic radii. The resulting molecular structures are similar to the traditional ball and stick ones, with the difference that in this model each object included in the plot provides topological information about the atoms and bonding interactions. As a result, the character and intensity of any given interatomic interaction can be identified by visual inspection, including the noncovalent ones. Because similar bonding interactions have similar plots, this tool permits the visualization of chemical bond transferability, revealing the presence of functional groups in large molecules.
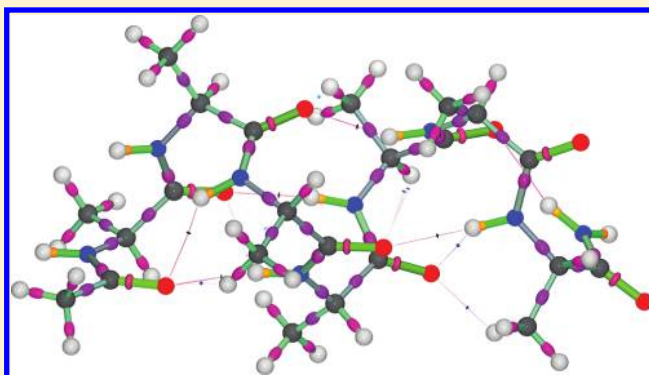
INTRODUCTION

The molecular structure hypothesis states that a molecule is a combination of atoms linked by an arrangement of bonds. The quantum theory of atoms in molecules (QTAIM)[1] offers a theoretical and computational framework to recover chemically meaningful graphs from the electron density and provides a physical basis for the development of mathematical representations of molecular structures. In QTAIM, the molecular graph is the collection of bond paths, i.e., lines of locally maximal electron density linking bonded nuclei, and the corresponding bond critical points.[1−3] The molecular graph and the physical properties at the bond critical points (BCPs) provide a precise account of the bonding within a molecule or crystal.[1−6] Therefore, it will be practical if such topological information is graphically included within the chemical structure. Unfortunately, the available molecular structure representations may not vividly reflect the bonding information provided by QTAIM. The present work is one of the first attempts to pursue such a goal.

The growing number of theoretically and experimentally studied molecular structures with QTAIM has resulted in an increasing need for tools for visualization and analysis.[6,7] In recent years, much improvement has been achieved in its implementation,[8,9] and several programs for QTAIM analysis are available, such as AIMPAC,[10] AIM2000,[11] MORPHY,[12] AIMAll,[13] and TOPXD,[14] among others. The visualization of the molecular graph, however, has remained essentially unchanged since the initial proposals for the molecular structure representation in terms of the topology of the electron density.[1−3]

In the present paper we show that the topological properties of the electron density at the critical points can be used to generate a new graphical representation of the molecular structure. The local behavior of the electron density at the critical points can be represented by ellipsoids that depend on the eigenvalues of the Hessian of the electron density. In addition, the bonds thicknesses can be scaled proportionally according to the electron density at the BCP, which facilitates the visual identification of strong and weak bonding interactions.

We implemented this idea in POV-Ray,[15] a cross-platform script language and rendering engine that is commonly used for generating high quality 3D graphics, including molecular structures. The program reads a standard output file from AIMAll, but the basic idea can be easily adapted for using output files produced by other QTAIM programs.

First, we demonstrate the need for a 3D representation of the critical points. Then we explicate how this idea is implemented in POV-Ray, and finally, we show the usefulness of this tool with a few selected examples.

METHODS

The molecular graph is a simplified representation of the chemical bonding, which is accounted for by the electron density.[16,17] Whereas the molecular graph is essentially a discrete representation, the electron density is a continuum, with a variety of features not captured by the usual representations of the

molecular graph. We have proposed the study of the logarithmic derivative of the electron density, $\tilde{p} = 1/2|\nabla ln\rho|$ (atomic units), as a practical tool for the identification of electronic regions in atoms and molecules.[18−20] While the study of $\tilde{p}$ applies to every point of the molecular space, the graphical representation presented here applies only to the critical points of the electron density, that it is a discrete representation of the molecular structure.

Around the stationary points of the electron density (i.e., the critical points $\nabla\rho = 0$), $\tilde{p}$ isocontours are simple-connected shapes that follow the local curvature of the electron density. Within the neighborhood of any critical point, $\tilde{p}$ goes to zero and the topology of the isocontours $\tilde{p} \sim 0$ is dominated by $|\nabla\rho| \sim 0$. (This is true in general for every function of the form $\nabla\rho/\rho^m$, as can be obtained by applying L'Hopital's rule to this ratio and using the fact that the electron density is a continuous function with continuous derivatives. Hence, it also applies to the unitless gradient study by Johnson et al. that is based on promolecular densities.[21]) From the analytical expansion of the electron density, the approximate expression of the gradient around a critical point $\mathbf{r}_0 = (x_0, y_0, z_0)$ is given in terms of the second derivatives by

$$\nabla\rho \approx (x - x_0)\lambda_1\mathbf{u}_1 + (y - y_0)\lambda_2\mathbf{u}_2 + (z - z_0)\lambda_3\mathbf{u}_3 \quad (1)$$

where $\{\lambda_1 \leq \lambda_2 \leq \lambda_3\}$ are the eigenvalues (or *principal curvatures*) of the Hessian, and $\{\mathbf{u}_i\}$ their respective eigenvectors (or *principal directions*); where $\mathbf{r} = (x, y, z)$ is the position vector near the critical point $\mathbf{r}_0$ and $|\mathbf{r} - \mathbf{r}_0| \rightarrow 0$. It is assumed that both position vectors are given in terms of the orthonormal basis set $\{\mathbf{u}_i\}$. After taking the square of the gradient vector (eq 1) and dividing by $|\nabla\rho|^2$, the equation of an ellipsoid centered at $\mathbf{r}_0$ is obtained
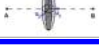
$$\frac{(x - x_0)^2}{a^2} + \frac{(y - y_0)^2}{b^2} + \frac{(z - z_0)^2}{c^2} \approx 1 \quad (2)$$

whose principal axis are given by $a = |\nabla\rho|/|\lambda_1|$, $b = |\nabla\rho|/|\lambda_2|$, and $c = |\nabla\rho|/|\lambda_3|$ (assuming that all the critical points are rank-three, i.e., $\lambda_i \neq 0$, for $i = 1-3$).

Equation 2 demonstrates that the isocontours $\tilde{p} \sim 0$ are essentially ellipsoids centered at the critical points that are aligned with the local principal directions. In other words, at the critical points, the eigenvalues of the Hessian can be translated into a graphical representation of the local symmetry of the electron density via the isocontours $\tilde{p} \sim 0$. Therefore, the topological properties of the electron density can be studied by the *shapes* of the scalar field $\tilde{p}$, thanks to the correspondence between the isocontours and the curvatures established by eq 2.

The two first curvatures (λ_1 and λ_2) indicate electronic charge accumulation in the perpendicular direction to the bond path, while the third one (λ_3) measures the charge concentration along the parallel direction. It is important to note that, while the traditional QTAIM classification of the critical points is based on the sign of the curvatures,[1] the curvature analysis proposed herein emphasizes their magnitudes.[20]

The ellipsoids given by eq 2 are aligned with respect to the local principal directions (i.e., the Hessian eigenvectors), and they provide information about the local symmetry of the electron density at the critical points. The electron density around the nuclei has spherical symmetry because the three curvatures are (almost) identical, that is, $a \approx b \approx c$ for nuclei with atomic number greater than one.[18−20,22] Only bonded hydrogen atoms show a significant departure from spherical symmetry around the nuclear attractor position, due to its lack of a core electronic shell.

| Type of bond	Laplacian	Axes relations	Graphical representation
Covalent shared	$\nabla^2\rho < 0$	$c > a, b$	
Covalent closed-shell	$\nabla^2\rho > 0$	$c < a, b$	
Noncovalent closed-shell	$\nabla^2\rho > 0$	$c \ll a \approx b$	

Figure 1. Classification of the bond critical points according to their curvatures. The corresponding ellipsoid axes given by eq 2 are plotted for a hypothetical molecule A−B. The bond path is indicated by the dashed line. The three eigenvectors of the Hessian, $\mathbf{u}_i$, determine the main curvature directions and are indicated in blue.

For the rest of the periodic table it is topologically justified to represent the atomic nuclei by spheres. It is important to note that the scalar field $\tilde{p}$ has removable discontinuities exactly at the nuclei, that is, at every nuclear position $\mathbf{R}_A$, $\tilde{p}(\mathbf{R}_A) = 0$, (because the electron density reaches a local maximum and hence the gradient vanishes), but $\tilde{p}(\mathbf{R}_A + \delta\mathbf{r}) = Z_A$, with $\delta\mathbf{r}$ a vector with infinitesimally small magnitude $|\delta\mathbf{r}| > 0$. It means that all the points in the neighborhood of the nucleus behave according to Kato's cusp condition.[23] The ellipsoid given by eq 2 also explains the spike-shaped ellipsoids found at the *ring critical point* (RCP) of benzene and similar structures, for which the curvatures on the plane are smaller than the perpendicular one, that is, $a \approx b \ll c$.[19,22]

In a previous publication it has been shown that $\tilde{p}$ correctly provides the atomic shell structure[18] and that the same variable defines an experimentally determined atomic radius that depends exclusively on the ionization energy.[24] These atomic radii are used for the representation of the atomic sizes in the present molecular model.

The magnitude of the local curvatures at the BCPs indicate the type of interaction between the interconnected nuclei.[20] As a consequence, the ellipsoid equation (eq 2) supplies a graphical representation for each kind of bonding interaction. For instance, a typical covalent bond is characterized by a third curvature smaller than the other two ($|\lambda_3| \ll |\lambda_{1,2}|$),[1] and hence, the associated ellipsoid has a cylindrical shape ($c > a, b$) whose main axis is aligned with the bond path linking the nuclei. Other types of covalent bonds have very large ionic-covalent resonance energies and they are characterized by a positive Laplacian. This type of bond has been termed *charge shift* by Shaik.[25] In this case, the corresponding ellipsoid has a spheroidal shape, because the third curvature is bigger than the other two ($|\lambda_3| > |\lambda_{1,2}|$), which means that the parallel axis is smaller than any of the perpendicular ones ($c < a, b$). Noncovalent interactions (i.e., van der Waals, hydrogen bonds, etc.) also have a positive Laplacian, but the value of the third eigenvalue is about one order of magnitude bigger than the other two,[1] ($|\lambda_3| \gg |\lambda_{1,2}|$), and therefore, the corresponding ellipsoids are discs perpendicular to the bond path, as has been discussed before.[20] A classification of the BCPs according to their corresponding ellipsoid shapes (as given by eq 2) is shown in Figure 1.

In summary, the saddle points of the electron density exhibit local characteristic symmetries that can be used for a molecular structure representation. For the bond critical points in particular, there are three main classes of interatomic interactions that can be visualized distinctively, namely, the covalent, closed shell and noncovalent interactions, and every bonding interaction falls within those classifications.
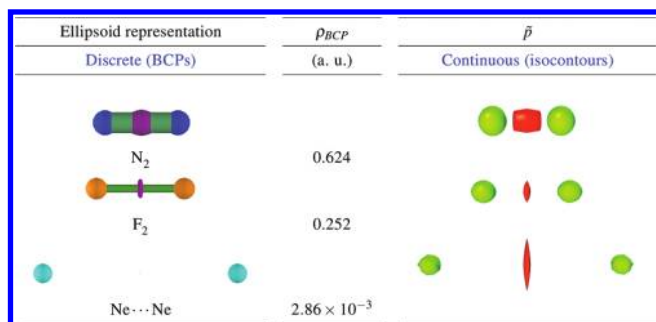
Figure 2. Discrete (left) vs continuous (right) representations of the bond critical points. The $\tilde{p}$ isocontours are 0.4 au (BCPs, orange) and 3.0 au (nuclei, green). The thickness of the bond paths are proportional to the electron density at the BCP, ρ_{BCP}.
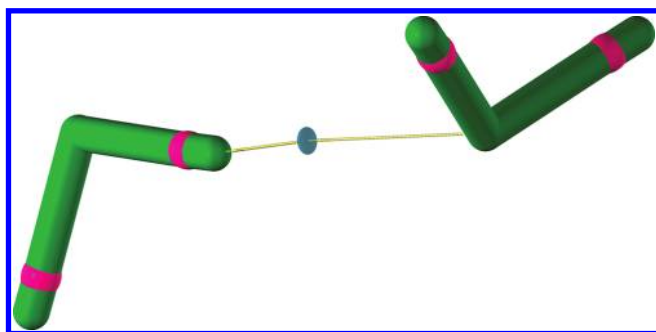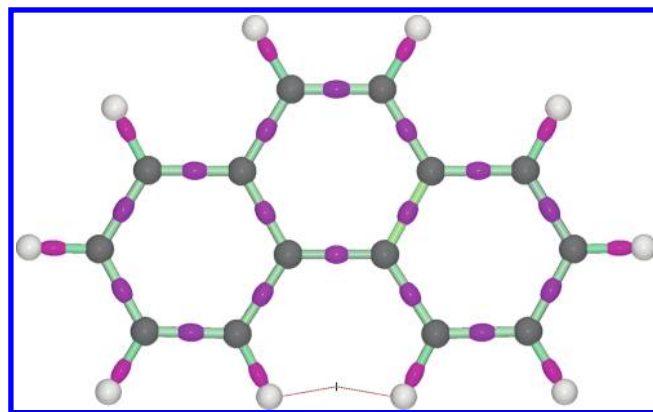

Figure 3. Discrete representation of the molecular structure of the water dimer.

Details of the Implementation. According to eq 2 the ellipsoid axes are proportional to the gradient of the density and inversely proportional to the curvatures. Since the gradient vanishes at the critical points, an alternative quantity for the numerator defining the ellipsoid axes is needed. We use the quantity $\rho\sqrt{\lambda}$, where λ is the geometric mean of the magnitude of the curvatures. (The geometric mean of three numbers, a, b, and c, is the length of one side of a cube whose volume is the same as that of a right cuboid with sides whose lengths are equal to the three given numbers.) Therefore, the axes are computed as $a = 3\rho\lambda^{1/2}/4|\lambda_1|$, $b = 3\rho\lambda^{1/2}/4|\lambda_2|$, and $c = 3\rho\lambda^{1/2}/4|\lambda_3|$.

Each critical point is represented by an ellipsoid centered at its coordinates, aligned with the principal directions, and scaled according to the values of a, b, and c. The geometric object used is called *a superellipsoid* because it provides a flexible range of continuous deformations for a basic shape. The superellipsoid object creates a shape known as a superquadric ellipsoid. It can be used to create boxes and cylinders with round edges and other similar shapes. Mathematically, it is given by the equation

$$f(x,y,z) = \left(|x|^{2/e} + |y|^{2/e}\right)^{e/n} + |z|^{2/n} - 1 = 0 \qquad (3)$$

where n and e are parameters, and the equation is fully implemented in POV-Ray. For $e = 1$, the object produced by this equation is a rounded cylinder (if $e = n = 1$, the object generated is a sphere), which is the one we need for the BCPs. Therefore, we use a single parameter to control the ellipsoid_shape. It is convenient to use the curvature quantity $n = \lambda/\bar{\lambda}$, with $\bar{\lambda}$ the arithmetic mean of the magnitude of the curvatures. A similar parameter was studied by Jenkins et al. in a very recent letter,

Figure 4. Discrete representation of the molecular structure of phenanthrene. The H−H interaction in the bay zone is weaker than a hydrogen bond.
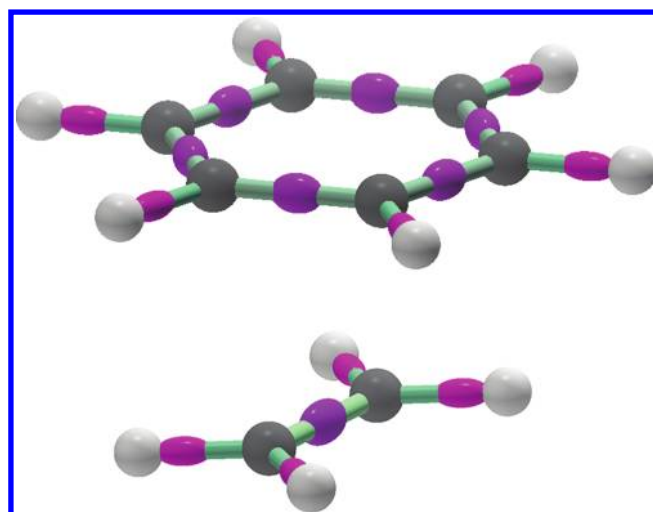

Figure 5. Discrete molecular representation of benzene and ethene. The C−C bonds of both molecules (in purple) have ellipticities, $\varepsilon > 0$, indicating their π character.

where the ratio of the strength of the tensile mode to the average of the compressive modes of the stress tensor is used to characterize charge-shift bonding without the risk of including metallic bonds like Li−Li in that category.[26]

In this representation, the bond paths are approximated by straight lines. The bond path joining two atoms is represented by a cylinder whose radius is directly proportional to the electron density $(\rho/2)$, which makes strong bonds look thicker than the weak ones. In addition, the bond paths for which $\nabla^2\rho > 0$ are made transparent, with the transparency level given by a function of the electron density at the BCP. The color of the bond paths depends on a function of the electron density and the curvatures. The color of the ellipsoids representing the BCPs is sensitive to the third curvature. Therefore, similar bonding interactions must give similar colors, and the corresponding bond paths must have similar thicknesses.

Finally, the nuclei are plotted as spheres with each radius equal to one-half the atomic radius given by the corresponding ionization energy I, according to which $r_o = (I_H/I)^{1/2}$, where I_H is the ionization of hydrogen.[24] The nuclei are colored according to the CPK standard code.
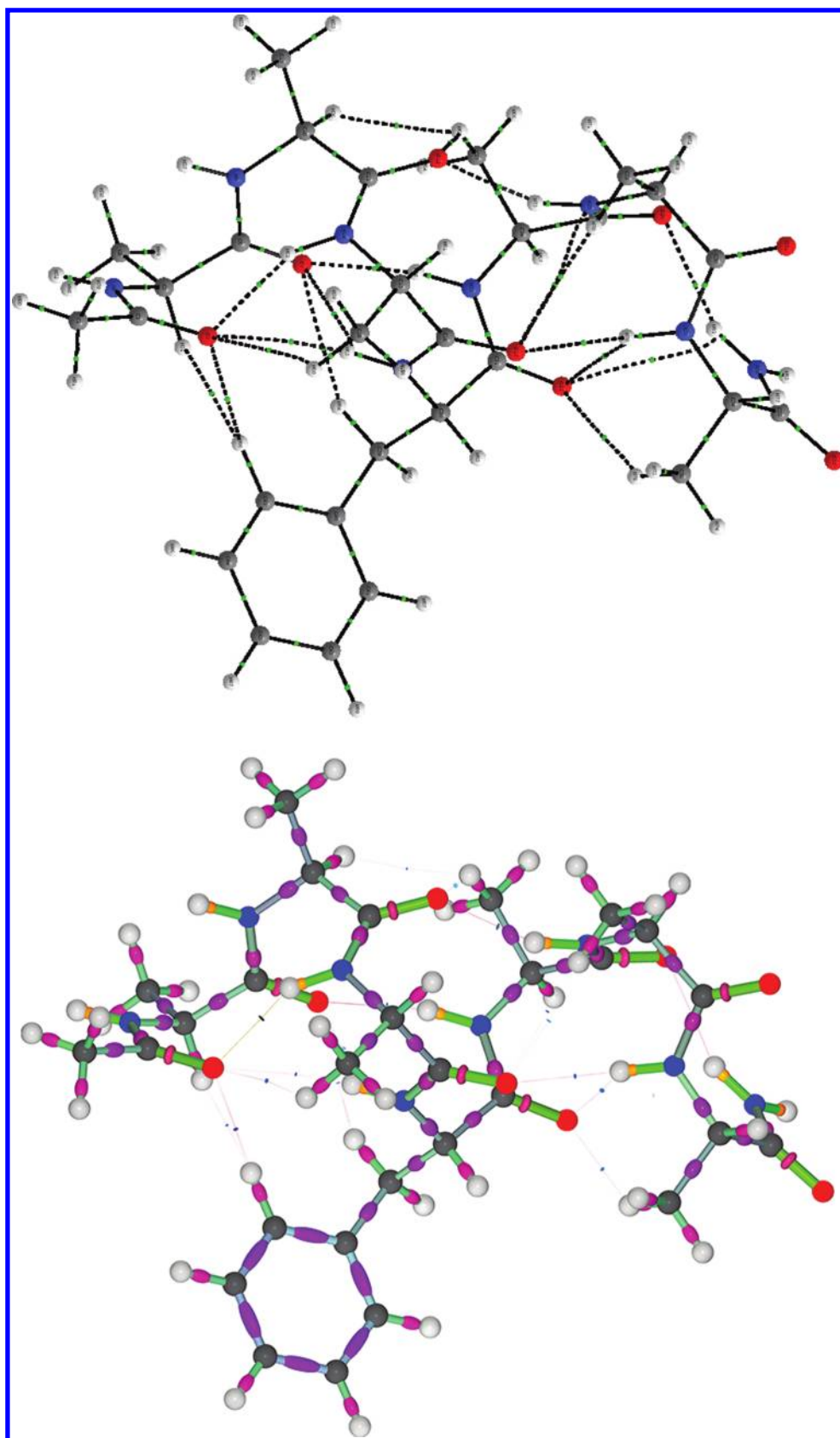
Figure 6. Polypeptide $COCH_3(Ala)_3Phe(Ala)_3NH_2$, as represented by the standard molecular graph (top) and according to the present proposal (bottom).

The critical points representation was created with a script written in AWK which is available by contacting the corresponding author.

The input files for generating the discrete molecular structures are the SUM files generated by AIMAll.

■ RESULTS

All computations were made at the MP2/cc-pVDZ level of theory (unless otherwise stated) by use of Gaussian09.[27]

We first describe the results of calculations on three simple test systems where comparison can be made with the continuous local curvatures given by the isocontours of $\tilde{p}$. These isocontours where obtained by use of Chimera[28] from cube grids produced from the wave function by Checkden,[29] as previously described.[19,20]

Figure 2 shows the ellipsoid representation of the BCPs for three diatomic molecules with different bonding interactions. These molecules exemplify the three cases of bonding interactions shown in Figure 1. The discrete representation keeps the essential features of the BCPs, as given by $\tilde{p}$, with the additional advantage that they are easier to compute. The ellipsoids representing the BCPs of the two covalent bonds are similar in size and shape to those given by the isocontours of $\tilde{p}$. The thickness of the bond paths are proportional to the electron density at the BCP, and hence, the discrete representation provides an intuitive idea of the strength of the bonding interactions involved. Accordingly, the bond path for the neon complex is practically invisible, a clear indication that the neon atoms are bonded by a much weaker interaction than the two covalent bonds. The respective ellipsoid is a disk perpendicular to the bond path and parallel to the interatomic surface, as expected.[20]

In the water dimer shown in Figure 3, the hydrogen bond is clearly depicted as a small disk joining the two water molecules by a thin line. The electron density at the O—H BCPs is $\rho \sim 0.38$ au, that is, a strong covalent bond, while for the hydrogen bond is just less than an order of magnitude smaller with $\rho \sim 2.54 \times 10^{-2}$ au. The graphical representation consistently shows these two types of bonding interactions.

The visualization of the topological information facilitates the comparison of chemical bonds. It is possible to visually compare two different molecular systems (provided that the level of theory is the same) in order to determine the kind of bonding interactions involved. For instance, Figure 4 shows the discrete molecular representation for phenanthrene whose bay zone reveals a BCP between two hydrogen atoms. These 'dihydrogen contacts' have received some attention recently as the theoretical and experimental evidence grows.[30,31] When compared with the hydrogen bond (Figure 3) it can be verified that the H—H interaction is a weaker interaction than the hydrogen bond but stronger than the one occurring in the neon dimer (Figure 1). In fact, the electron density for the H—H BCP is $\rho \sim 1.30 \times 10^{-2}$ au, that is, almost one-half the density for the hydrogen bond BCP in the water dimer, but almost five times larger that the electron density at the BCP of the neon dimer. The graphical description agrees with chemical intuition for the system, i.e. that while the hydrogen atoms at the bay region are interacting effectively, its interaction is weaker than that one of a hydrogen bond (i.e., the dihydrogen contact is "subtle but not faint"[31]).

Three decades ago, Bader et al. proposed to measure the departure of a bond path from cylindrical symmetry by the now well-known ellipticity ε.[32] The ellipticity, $\varepsilon = \lambda_1/\lambda_2 - 1$ (or $\varepsilon = b/a - 1$, in terms of the ellipsoid axes), indicates the π character of the bonding interactions. The ellipticities ε for the C—C bonds of benzene and ethene are 0.21 and 0.35, respectively, which is consistent with their π nature. In Figure 5 these bonds appear as purple ellipsoids revealing the axial asymmetry that results from $\varepsilon > 0$ (or $b > a$). The ethene double bonds have a greater asymmetry around the bond paths than the aromatic bonds of
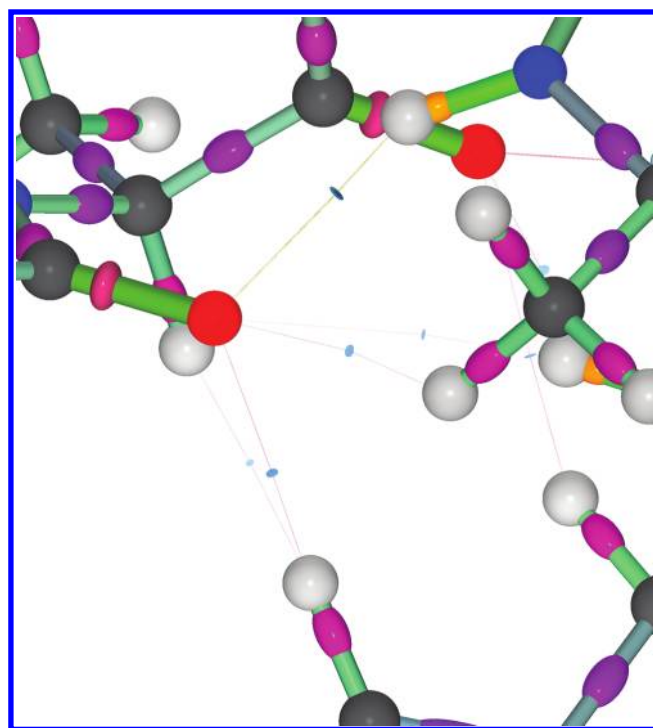

Figure 7. Detail of Figure 6 showing the bond paths emerging from the oxygen to the left.

benzene, which is consistent with the values of ε. Notice the similarity in colors and shapes of these two molecules with that of the phenanthrene in Figure 4. This agreement reflects (visually) the high degree of transferability of the topological parameters characterizing the chemical bonds.[33]

A few final examples illustrate the utility of the present molecular representation for the study of large, complex systems. In particular, inside biological molecules there are hundreds of bonding interactions of all types, which complicates its topological analysis. Figure 6 shows the polypeptide $COCH_3(Ala)_3Phe(Ala)_3NH_2$ in the α-helix conformation (obtained at B97D/D95(d,p) level of theory, with solvent effects simulated by PCM (water)). The conventional molecular graph (top of Figure 6) reveals several bond paths emerging from the electronegative atoms, and it is not clear from the graphic which ones are hydrogen bonds and which ones are just topological contacts. It may also be difficult to follow the 3D structure from the molecular graph alone.

On the other hand, the discrete representation of the peptide shown at the bottom of Figure 6 provides a clear distinction of the involved functional groups such as the phenyl group of the phenylalanine, the methyl groups of the alanines, and the peptide bonds, for instance. While all the C—H bonds are identical (in pink), the C—C bonds of the aromatic ring are longer than those of the sp^3 carbons; nevertheless, the thickness of the bond paths is very similar for all C—C interactions, which indicates a similar electron density at those BCPs. In fact, the electron density at the C—C BCPs is almost constant, with $\rho \sim 0.25$ au. In a similar way, from the graphic, it can be inferred that the C—O and N—H bonds have similar densities (indeed, $\rho \sim 0.37$ and $\rho \sim 0.34$ au, respectively) but very different local symmetries (in dark pink and yellow, respectively).

In addition, the intramolecular hydrogen bonds are distinguished from the other interconectivities emerging from the
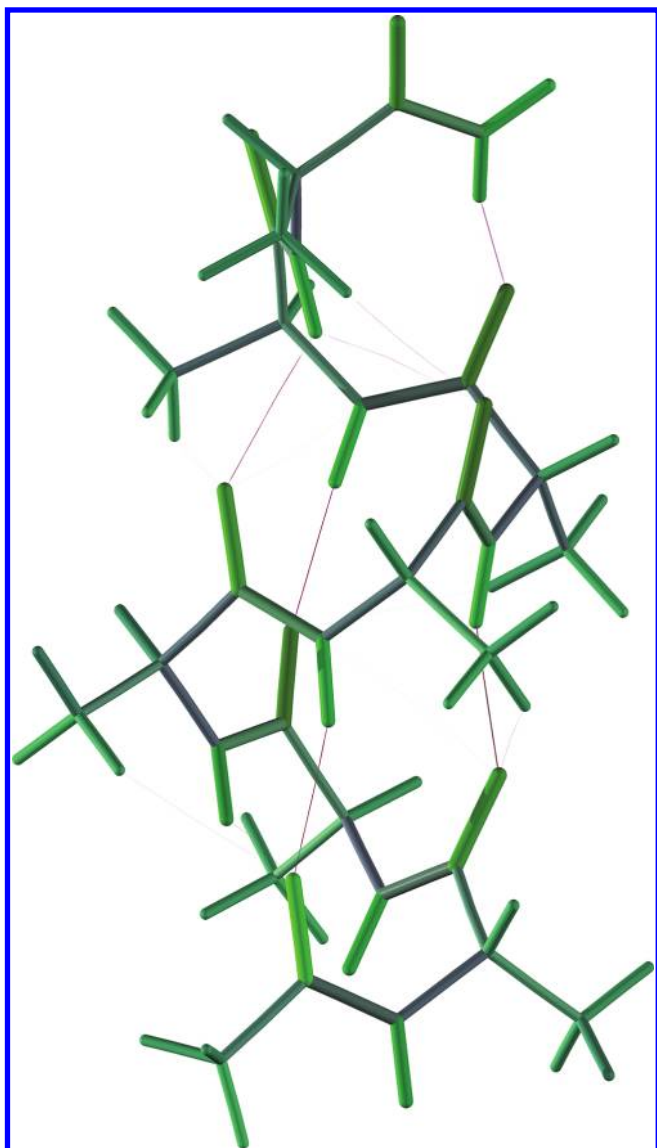
Figure 8. Polyalanine peptide $(COCH_3(Ala)_7NH_2)$ in the α-helix conformation. Only the bond paths are plotted. The thickness is proportional to the electron density at the respective BCP, and the color depends on the curvatures.

oxygen and nitrogen atoms, as shown in a closer inspection of the same molecule in Figure 7. Comparison of all the bond paths emerging from the oxygen atom shows that the one pointing to the top-right is more visible among the others, indicating that such a BCP is associated with a true intramolecular hydrogen bond ($\rho \sim 2.17 \times 10^{-2}$ au). The remaining topological contacts have smaller (about 30%) electron densities and hence less chemical relevance ($\rho \sim 7.27 \times 10^{-3}$ au in average). Nevertheless, these noncovalent contacts have a cumulative stabilizing effect, similar to the amide N and carbonyl O atomic contacts found in larger polypeptide helices ($N \cdots O$), as recently proposed by the authors.[34]

By plotting only the bond paths of a polyalanine peptide ($COCH_3(Ala)_7NH_2$; the level of the theory used is the same as the previously mentioned peptide), it is clear that it captures the α-helix secondary structure pattern given by the hydrogen bonds, as shown in Figure 8. This molecular feature is the result of the combined effect of covalent and hydrogen bonds. Hence,

the secondary structure pattern only emerges by simultaneously comparing all the involved bonding interactions.

CONCLUSIONS

We have tested the idea that it may be advantageous to get a translation of the topological information provided by QTAIM into the form of a molecular structure. This new representation of molecular systems depicts three-dimensionally the topological information of the critical points. With this graphical tool it is possible to visualize the strength and, in part, the nature of any given atomic interaction, as characterized by a set of basic properties of the BCPs. It facilitates distinguishing the types of interatomic interactions, in particular noncovalent ones from stronger ones. Hydrogen bonds are distinguished from weaker interatomic contacts, such as dihydrogen contacts and other noncovalent interactions.

The critical points are represented by ellipsoids, in complete agreement with previous studies on the curvatures of the electron density around the critical points.[19,20,22] One feature that is usually hard to visualize in QTAIM is the transferability of bonding interactions. The discrete molecular representation visualizes similar bonds in a similar way because it reflects the values of the curvatures at the BCPs by the color and shape of the ellipsoids and the electron density by the thickness of the bond path. This topologically based representation of molecules may facilitate the study of functional groups and hydrogen bonds in large and complex systems.

In summary, it has been shown that the theory of atoms in molecules gives rise to a practical quantum definition of molecular structure. The resulting molecular structures are similar to the traditional ball and stick ones, with the difference that, in this model, each object included in the plot provides topological information about the atoms and chemical bonds. The present work is an attempt to improve the molecular representation in a way that reflects the quantum topology of the chemical bond. This tool may be suitable for the study of molecular complexes and nano-structures, which include several types of bonding interactions, ranging from covalent to noncovalent ones.

AUTHOR INFORMATION

Corresponding Author
*E-mail: hugo.j.bohorquez@dal.ca.

REFERENCES

(1) Bader, R. F. W. *Atoms in Molecules. A Quantum Theory*; Oxford University Press: Oxford, England, 1990.

12996

dx.doi.org/10.1021/jp204100z |*J. Phys. Chem. A* 2011, 115, 12991–12997

(2) Nguyen-Dang, T. T.; Bader, R. F. W. *Phys. A* **1982**, *114*, 68–73.

(3) Popelier, P. L. A. *J. Phys. Chem. A* **1999**, *103*, 2883–2890.

(4) O'Brien, S.; Popelier, P. *Can. J. Chem.* **1999**, *77*, 28–36.

(5) Gatti, C. *Z. Kristallogr.* **2005**, *220*, 399–457.

(6) *The Quantum Theory of Atoms in Molecules. From Solid State to DNA and Drug Design*; Matta, C. F., Boyd, R. J., Eds.; Wiley-VCH: New York, 2007.

(7) *Quantum Biochemistry*; Matta, C. F., Ed.; Wiley-VCH: New York, 2010.

(8) Henkelman, G.; Arnaldsson, A.; Jónsson, H. *Comput. Mater. Sci.* **2006**, *36*, 354–360.

(9) Rodríguez, J. I.; Bader, R. F.; Ayers, P. W.; Michel, C.; Götz, A. W.; Bo, C. *Chem. Phys. Lett.* **2009**, *472*, 149–152.

(10) Biegler-Konig, F.; Bader, R.; Tang, T. *J. Comput. Chem.* **1982**, *3*, 317.

(11) Biegler-König, F.; Schönbohm, J. *J. Comput. Chem.* **2002**, *23*, 1489–1494.

(12) Popelier, P. L. A. *Comput. Phys. Commun.* **1996**, *93*, 212–240.

(13) Keith, T. A. *AIMAll*, Version 10.06.21; 2010, aim.tkgristmill.com.

(14) Volkov, A.; Gatti, C.; Abramov, Y.; Coppens, P. *Acta Crystallogr., Sect. A* **2000**, *56*, 252–258.

(15) *Persistence of Vision Raytracer*, Version 3.6; http://www.povray.org/download/

(16) Feynman, R. P. *Phys. Rev.* **1939**, *56*, 340–343.

(17) (a) Runtz, G. R.; Bader, R. F. W.; Messer, R. R. *Can. J. Chem.* **1977**, *55*, 3040–3045. (b) Bader, R. F. W. *J. Phys. Chem. A* **1998**, *102*, 7314–7323.

(18) Bohórquez, H. J.; Boyd, R. J. *J. Chem. Phys.* **2008**, *129*, 024110.

(19) Bohórquez, H. J.; Boyd, R. J. *Theor. Chim. Acc.* **2010**, *127*, 393–400.

(20) Bohórquez, H. J.; Matta, C. F.; Boyd, R. J. *Int. J. Quantum Chem.* **2010**, *110*, 2418–2425.

(21) Johnson, E. R.; Keinan, S.; Mori-Sánchez, P.; Contreras-García, J.; Cohen, A. J.; Yang, W. *J. Am. Chem. Soc.* **2010**, *132*, 6498–6506.

(22) Bohórquez, H. J. *Ph.D. Thesis*, Dalhousie University: Halifax, Nova Scotia, Canada, 2011.

(23) Kato, W. A. *Commun. Pure Appl. Math.* **1957**, *10*, 151–177.

(24) Bohórquez, H. J.; Boyd, R. J. *Chem. Phys. Lett.* **2009**, *480*, 127–131.

(25) Shaik, S.; Danovich, D.; Wu, W.; Hiberty, P. C. *Nat. Chem.* **2009**, *1*, 443–449.

(26) Jenkins, S.; Kirk, S. R.; Guevara-García, A.; Ayers, P. W.; Echegaray, E.; Toro-Labbe, A. *Chem. Phys. Lett.* **2011**, *510*, 18–20.

(27) Frisch, M. J. et al. *Gaussian 09*, Revision A.1; Gaussian, Inc.: Wallingford, CT, 2009.

(28) Pettersen, E. F.; Goddard, T. D.; Huang, C. C.; Couch, G. S.; Greenblatt, D. M.; Meng, E. C.; Ferrin, T. E. *J. Comput. Chem.* **2004**, *13*, 1605–1612.

(29) Pacios, L. F.; Fernandez, A. *J. Mol. Graphics Modell.* **2009**, *28*, 102–112.

(30) (a) Matta, C. F. In *Hydrogen Bonding-New Insight* (Challenges and Advances in Computational Chemistry and Physics Series); Grabowski, S., Ed.; Springer: Netherlands, 2006; pp 337−376. (b) Matta, C. F.; Hernández-Trujillo, J.; Tang, T.-H.; Bader, R. F. W. *Chem. Eur. J.* **2003**, *9*, 1940–1951.

(31) Echeverria, J.; Aullon, G.; Danovich, D.; Shaik, S.; Alvarez, S. *Nat. Chem.* **2011**, *3*, 323–330.

(32) Bader, R. F. W.; Slee, T. S.; Cramer, D.; Kraka, E. *J. Am. Chem. Soc.* **1983**, *105*, 5061–5068.

(33) Bader, R. F. W.; Becker, P. *Chem. Phys. Lett.* **1988**, *148*, 452–458.

(34) LaPointe, S. M.; Farrag, S.; Bohorquez, H. J.; Boyd, R. J. *J. Phys. Chem. B* **2009**, *113*, 10957–10964.

12997

dx.doi.org/10.1021/jp204100z |*J. Phys. Chem. A* 2011, 115, 12991–12997